

Article

Two Case Studies of the Northwestern Argentinean Low: With and without a Coupled Transient Trough

Josefina M. Arraut ^{1,*}, Maurício R. Rocha ^{1,2}, Enio P. Souza ¹ and Júlia Amanda Nanini ¹

¹ Department of Atmospheric Sciences, Federal University of Campina Grande, Campina Grande 58436, Brazil; mauricio.rocha@usp.br (M.R.R.); enio.souza@ufcg.edu.br (E.P.S.); julia.amanda@estudante.ufcg.edu.br (J.A.N.)

² Oceanographic Institute of the University of São Paulo, São Paulo 20520, Brazil

* Correspondence: josefina.arraut@ufcg.edu.br

Abstract: The Northwestern Argentinean Low (NAL) intensifies the zonal component of the geopotential gradient to its east, intensifying the meridional wind and moisture flow from the tropics to the subtropics contributing importantly to the South American Low-Level Jet and the Chaco Jet. This study compares two situations where the NAL is present in the continent's subtropics: one where it is coupled with an extratropical transient trough to its south and another without this coupling. The coupled case, called the front case, is stronger in two ways: it is warmer and shows lower geopotential at the center of the NAL. It also shows much stronger moisture transport. Both cases show a similar trait in that moisture transport and the zonal component of the geopotential gradient east of the NAL peak in the coolest hours. The geopotential at the center of the no-front case remains roughly constant throughout the event. For the front case, it attains its minimum value in the six hours preceding the northeastward advance of the transient trough. These results suggest that there are different mechanisms acting at the center of the NAL and at its eastern branch, as well as in the front and no-front cases.



Citation: Arraut, J.M.; Rocha, M.R.; Souza, E.P.; Nanini, J.A. Two Case Studies of the Northwestern Argentinean Low: With and without a Coupled Transient Trough. *Atmosphere* **2023**, *14*, 883. <https://doi.org/10.3390/atmos14050883>

Academic Editor: Arkadiusz Marek Tomczyk

Received: 17 February 2023

Revised: 2 March 2023

Accepted: 10 March 2023

Published: 18 May 2023



Copyright: © 2023 by the authors. Licensee MDPI, Basel, Switzerland. This article is an open access article distributed under the terms and conditions of the Creative Commons Attribution (CC BY) license (<https://creativecommons.org/licenses/by/4.0/>).

1. Introduction

The South American southern summer climatology features a long, narrow, meridional band of low-pressure east of the Andes in the lower tropospheric levels [1–3]. This band is quasi-permanent, extending from Northern Argentina to the Southern Amazon, and contains two local minima (see Figure 1). One of these local minima is centered around 20° S and is known as the Chaco Low (CHL), whereas the other one is centered around 29° S and is called the Northwestern Argentinean Low (NAL) (Figure 1) [4–7].

For both of these lows, sensible heating from the ground is essential but the CHL is also forced by latent heating from thunderstorms [3,5]. During winter, only the NAL occurs albeit intermittently [4,8]. There is evidence that the winter cases are forced by the Zonda Wind [9], a local name for the Fohn Effect, which occurs when the high-level subtropical jet intensifies over the Andes [4,10].

The low-pressure meridional band, which includes the NAL and CHL, plays a key role in the weather and climate of South America. In the context of the South American monsoon system, this band has the same role as the East Asian summer monsoon trough, helping to bring moisture flow from the ocean into the continent [1,5]. The Gran Chaco region itself is divided into Boreal Chaco, which is warm and dry, and a cooler and wetter Oriental Chaco [11], which is under the influence of thunderstorms and mesoscale convective complexes (MCC) that form in the exit region of the South American Low-Level Jet (SALLJ). These two regions correspond to rainfall clusters R3 and R4, respectively, as discussed in [12]. R3 has overall less rainfall throughout the year and a pronounced dry season from June to August, whereas R4 has more rain and a lower amplitude in

its seasonal cycle. The NAL is instrumental in strengthening and extending meridional moisture transport toward the subtropics and extratropics. The intensification of the NAL is the primary mechanism for the production of the Chaco Jet (CHJ), which is known as a southward extension of the SALLJ [13–15]. The intensification of moisture transport toward the subtropics is strongly linked to subtropical rainfall. MCC are 17 times more common when the CHJ occurs than on days when it does not [15].

The intensification of the NAL is concomitant with a significant increase in the equivalent potential temperature in the South American subtropics (see [4,6]) and this increase is important for both frontogenetic and cyclogenetic processes [6,16]. According to [16], cyclogenesis typically occurs off the coast of South America at around 40° S. This process is preceded by the formation of an entropy reservoir to the northwest, which is characterized by high values of equivalent potential temperature.

Some works mention the NAL as having a strong diurnal cycle [4,7]. However, Ref. [6] explores the coupling between the low and transient troughs coming from the Pacific and indicates that the NAL's most prominent cycle is in the synoptic time scale, intensifying and dissipating over three or four days. These transient troughs move eastwards, crossing the Andes. Once the trough axis is east of the Andes, the mid-latitude air flowing along its western branch approaches the warm moist tropical air that flows along the eastern branch of the NAL. Very strong frontogenesis in the equivalent potential temperature occurs, especially at the Argentinean Col [6,17,18]. The environment becomes very baroclinic and the transient trough intensifies and grows in size. Heavy rainfall occurs along the frontal region between the two air masses. The growth of the trough, combined with its eastward displacement, causes the mid-latitude air and frontal region to advance northeastward, producing cold advection that dissipates the NAL from the south [6,19]. Comparing the NAL's behavior in the presence and absence of a coupled transient trough is an important step toward shedding light on the mechanisms causing subtropical rainfall in South America.

Despite the prominent role of the NAL in South American weather and climate, it has been the focus of very few studies over the last decade. In [4], two case studies of the NAL are compared: one in the warm and one in the cold season. This work, on the other hand, compares two warm season episodes, one with and one without a coupled transient trough, which are henceforth referred to as the front case and the no-front case. The aim is not to characterize the different behaviors systematically but rather to serve as a proof of concept for the existence of qualitative differences that merit further study. The question of whether the two behaviors correspond to different stages of the NAL's life cycle may arise. However, the NAL is quasi-permanent during summer and typically dissipates only with cold air incursions. For this reason, it may not be sufficient to consider separate NAL events but rather to understand that different patterns of behavior may emerge from the presence or absence of extratropical influences [2]. Moisture transport and rainfall are analyzed in both situations. As we will demonstrate, the differences between the two cases are sufficiently relevant to consider them qualitatively different. The front case, which has higher meridional moisture transport, shows lower rain rates. This is attributed to a previous drying of subtropical air because of a cold incursion. Overall, the no-front case shows a typically subtropical behavior, with rainfall responding mainly to the moisture flow convergence at the exit region of a tropical moisture flow. In contrast, the front case behaves in an extratropical manner, with rainfall along the front but a maximum over the Argentinean Col and is fed by moisture from the tropics.

Climate change studies show a poleward shift of the global monsoons, as well as an intensification of precipitation on the poleward side of monsoon regions. Precipitation in the equatorward side of the South American summer monsoon is projected to decrease while an increase is projected to occur in the low-pressure meridional band [20–22]. The Amazon is projected to show an increase in the number of consecutive dry days and a decrease in the number of consecutive wet days. The South Atlantic Subtropical High (SASH) is projected to undergo a slight southward shift and a slight strengthening because of the expansion of the Hadley Cell [20]. The same effects are projected for the South

Atlantic Convergence Zone (SACZ). These shifts may cause drying in central Brazil and a strengthening in convective activity in the subtropics [23]. A better understanding of precipitation mechanisms in the SACZ region and subtropical South America may aid the prediction of extreme events (see, for instance, [24]).

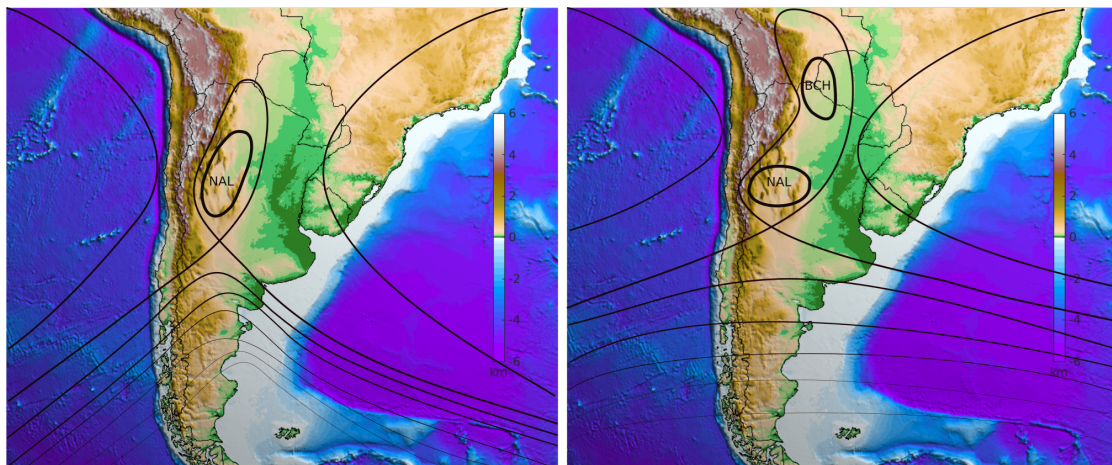


Figure 1. Schematic representations of the low-pressure tongue east of the Andes. The black contours represent the geopotential height and the colors show the topography in km. The left panel shows a situation in which the low-pressure tongue is coupled to a transient trough that has just passed over the Andes. The Northwestern Argentinean Low (NAL) is strong and is the only closed low within the low-pressure tongue. The right panel shows a situation where the low-pressure tongue has two lows inside of it: the NAL and the Chaco Low (CHL).

2. Materials and Methods

This study uses 6-hourly data from the European Centre for Medium-Range Weather Forecasts' (ECMWF) ERA5 reanalysis for the southern summer of 2016 (December 2015 to March 2016), which were retrieved from the Copernicus Climate Change Service (C3S) Climate Data Store public data server (<https://cds.climate.copernicus.eu/>), accessed on 24 December 2022). Local time is Universal Time Coordinated (UTC) + 3 h, so the data used were for 03, 09, 15, and 21 local times. The study also uses 3-hourly Tropical Rainfall Measuring Mission (TRMM) (<https://trmm.gsfc.nasa.gov/>, accessed on 12 December 2017) precipitation data and infra-red satellite imagery from GOES-13 (<https://www cptec.inpe.br/>, accessed on 18 December 2017).

The selection of two NAL cases during the southern summer of 2016, one with and one without a coupled transient trough and front was based on the 850 mb temperature and geopotential fields. The six-hourly data were visually inspected. Several other meteorological variables were used in the analysis, some of which were calculated. These variables are 850 mb winds, precipitation, vertically integrated moisture transport and its convergence, and the intensities of the zonal component of the geopotential gradient and the wind. Figures not showing the geopotential height have the position of the low-pressure tongue east of the Andes indicated by an actual geopotential height contour, which is only for reference. The contours have different values, which are not shown, in each panel.

Precipitable water (P_w) was computed from the surface (S_p) to 300 hPa as in [25]:

$$P_w = \frac{1}{g} \int_{S_p}^{300} q dp, \quad (1)$$

where q is the specific humidity in kg kg^{-1} and g is the Earth's gravitational acceleration (9.80655 m s^{-2}).

To calculate the equivalent potential temperature (θ_e) in K, we used the following equation [25]:

$$\theta_e = T \left(\frac{1000}{p} \right)^{0.2854 (1 - 0.00028 M_r)} \exp \left[\frac{3.376}{TL} - 0.00254(1 + 0.00081 M_r) M_r \right], \quad (2)$$

where T is the temperature in K, p is the pressure in hPa, M_r is the mixing ratio in g kg^{-1} , and TL is the temperature of the condensing level in K. The following equation was used to calculate M_r :

$$M_r = \left(\frac{0.622 e}{p - e} \right) 1000, \quad (3)$$

where e is the vapor pressure in Pa, which was computed as follows:

$$e = \frac{q p}{0.622 + 0.38 q}, \quad (4)$$

where q is the specific humidity in kg kg^{-1} . Finally, we computed TL in K using the equation:

$$TL = \frac{1}{\frac{1}{T-55} - \frac{\ln(\frac{r}{100})}{2840}} + 55, \quad (5)$$

where r is the relative humidity as a %.

The vertically integrated moisture transport (\vec{Q}) in $\text{kg m}^{-1} \text{s}^{-1}$ was calculated from the surface to 300 mb as follows:

$$\vec{Q} = \frac{1}{g} \int_{S_p}^{300} q \cdot \vec{V} dp, \quad (6)$$

where \vec{V} is the horizontal component of the wind velocity in m s^{-1} . We applied the horizontal component of the nabla operator ($\vec{\nabla}_H$) to obtain the divergence of the moisture transport in $\text{kg m}^{-2} \text{s}^{-1}$ using finite differences as follows:

$$DQ = \vec{\nabla}_H \cdot \frac{1}{g} \int_{S_p}^{300} q \cdot \vec{V} dp. \quad (7)$$

The geopotential field in $\text{m}^{-2} \text{s}^{-2}$ was converted into the geopotential height in meters by dividing it by g .

3. Results

Figures 2 and 3 show the temperature, geopotential height, and horizontal wind. At the center of the NAL, the difference between the lowest and warmest temperatures was 2°C for both events. However, the front case showed a warmer NAL, which remained warmer than its surroundings, even during its coolest hours. In the no-front case, the nightly cooling left the NAL very similar in temperature to its surroundings. The geopotential height field in the no-front case showed a low-pressure tongue at 1500 m at 18Z on 2 January. There was a slight strengthening of the pattern to 1480 m and 1460 m throughout the following 30 h.

The front case showed a weak high east of the Andes at 18Z on 23rd January due to a previous incursion of a transient high (not shown). At 00Z on 24th January this high has moved eastward. A strengthening of the NAL occurred in the following hours until 18Z on 24 January, reaching 1400 m. At 00Z on 25 January, the center of the NAL showed a slight weakening, with the geopotential height increasing to 1420 m. This took place while the front began to displace to the northeast, eroding the NAL from the south. These observations indicated that synoptic time scale variability was more important than diurnal variability in the front case.

Figures 4 and 5 show the magnitude of the zonal component of the geopotential gradient, as well as the wind intensity. In the subtropics, both these quantities were much stronger in the front case. A similarity, however, was that both cases peaked in the cool hours at 06Z and 12Z on 3 January and 06Z and 12Z on 24 January.

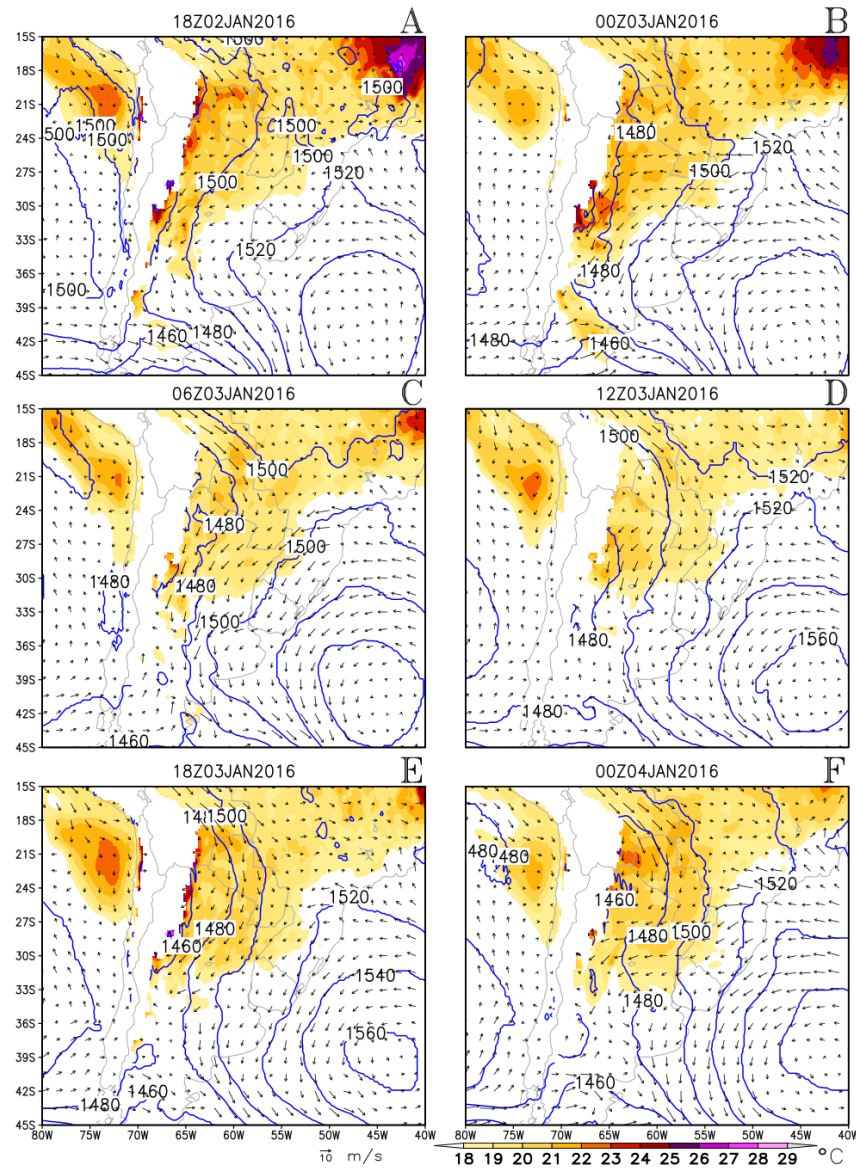


Figure 2. No-front case: Temperature values above 18°C (colors), wind (m s^{-1}) (vectors), and the geopotential height (contours) at intervals of 20 m at 850 mb. Panels (A–F) show different times, as specified above each panel.

3.1. Synoptic Analysis

The no-front case showed an elongated trough extending from the subtropics around 35° S of the tropics at around 18° S (Figure 3). The minimum geopotential height of the core of this elongated trough was between 1480 m and 1460 m from 00Z on 3 January until 00Z on 4 January. East of the NAL, the horizontal component of the geopotential height gradient and wind magnitude peaked during the cool hours at 06Z and 12Z on 3 January, as mentioned above. The Argentinean Col that separates the NAL from the westerlies to its south [6,17,19] was positioned roughly between 36° S and 39° S and between 70° W and 65° W throughout the studied period. At 18Z on 3 January 2016 and 00Z on 4 January 2016, the tip of a transient trough appeared south of the Col, causing it to shift slightly northward

by a couple of degrees. However, this trough showed no northward displacement between these two times. The SASH was centered at around 42° S during the whole event, which was south of its climatological position. The western branch of the SASH straddled the South American coast and there was confluence with the flow in the eastern branch of the trough at 18Z on 3 January 2016 and 00Z on 4 January 2016.

Meanwhile, the front case also showed an elongated trough reaching into the tropics but with a stronger minimum, which was the stronger NAL. The core of the NAL intensified until 18Z on 24 JAN, reaching 1400 m. East of the NAL, as mentioned above, the zonal component of the geopotential gradient and horizontal wind speed peaked in the cool hours at 06Z and 12Z on 24 January. From 18Z on 23 January 2016 to 06Z on 24 January 2016, the Argentinean Col moved southward from around 31° S to around 38° S as the NAL intensified. An extratropical transient trough coming from the Pacific appeared over the continent at 12Z on 24 January 2016. It intensified and the southwesterlies to the west of the trough advanced into the subtropics, causing temperatures to drop sharply. The NAL shrank toward the north and the Argentinean Col migrated northward correspondingly, as described in [6]. This is strong evidence that cold advection acted to dissipate the southern part of the NAL, which is in agreement with [4].

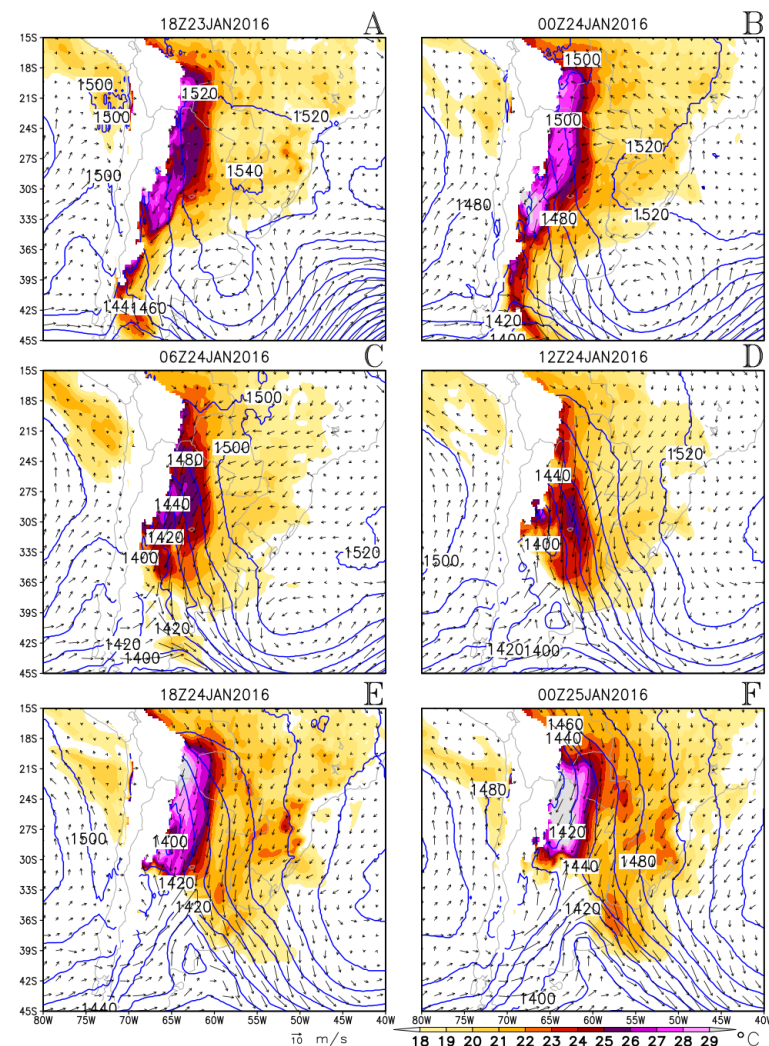


Figure 3. As in Figure 2 but for the front case. Panels (A–F) show different times, as specified above each panel.

3.2. Winds and the Geopotential Height Gradient

The no-front case (Figure 4) showed a tropical maximum in windspeed from about 20° S to 15° S, exceeding 12 m s⁻¹. In the subtropics, from 39° S to about 27° S, there was a second wind maximum, a CHJ, with an early morning peak at 06Z on Jan 03rd, of both quantities (see panel C). The front case (Figure 5) did not show the deeply tropical peak. However, it peaked at the same time in the subtropics and also a bit more intensely at 12Z on Jan 24th, reaching above 28 m s⁻¹. The front case showed very intense wind and zonal geopotential gradient values in the mid-latitudes at around 45° S on the eastern branch of the transient trough. Both the wind and the zonal component of the geopotential gradient were much stronger in the front case than in the no-front case.

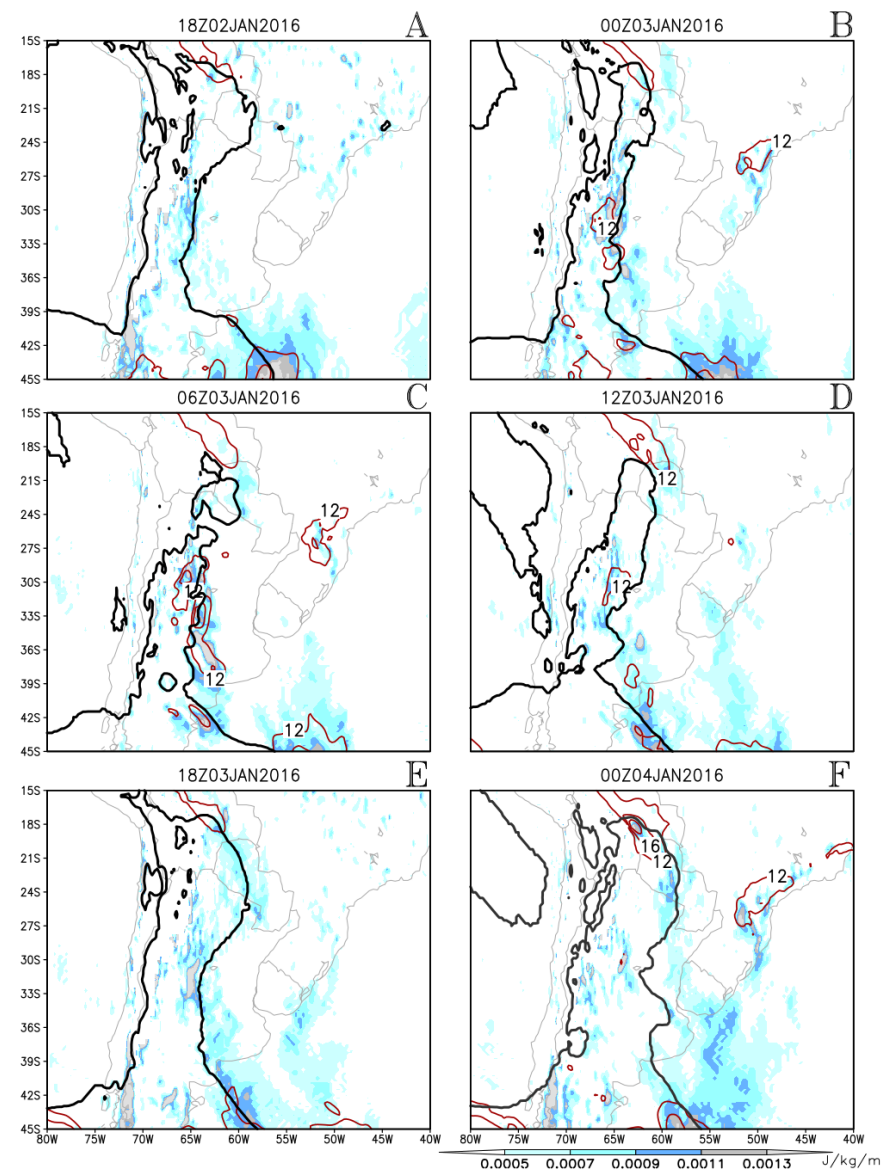


Figure 4. No-front case: Magnitude of the zonal component of the geopotential gradient at 850 mb. Values above $0.5 \times 10^{-3} \text{ J kg}^{-1} \text{ km}^{-1}$ are indicated by colors. Wind magnitude with values above 12 m s⁻¹ is indicated by the red contours at 850 mb. For reference, the position of the low-pressure tongue is indicated by an actual geopotential height contours in each panel. Panels (A–F) show different times, as specified above each panel.

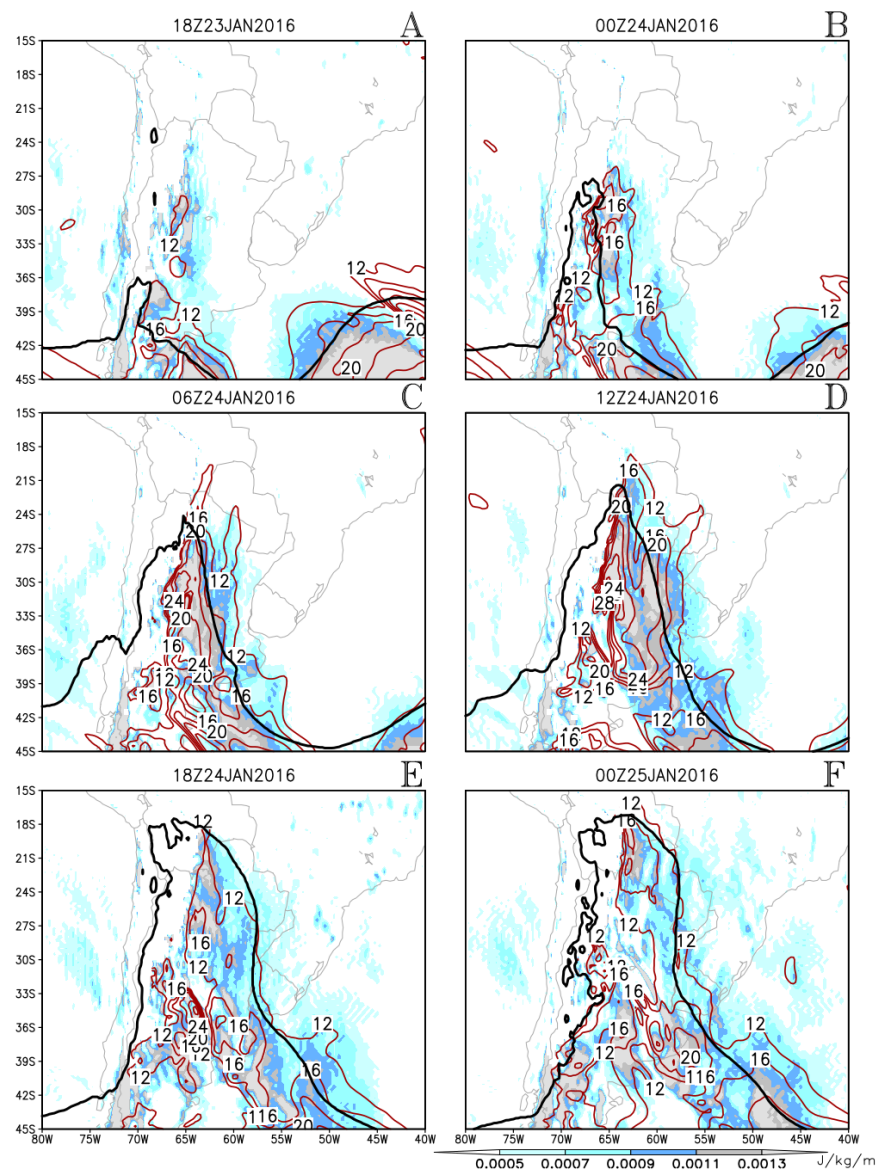


Figure 5. As in Figure 4 but for the front case.

The phase lock between the wind magnitude and zonal component of the geopotential gradient in the subtropics is an indication of the importance of geostrophic adjustment in this context. It is interesting to note that in both cases, these quantities peaked at night. This is in contrast to the geopotential at the center of the NAL, which was almost constant for the no-front case but was lowest at 18Z on January the 24th (3 p.m. local time) for the front case. This suggests two things, which are the topic of further study:

1. The geopotential at the NAL's center and its eastern branch responded to different physical mechanisms.
2. There were distinct physical mechanisms affecting the behavior of the geopotential at the NAL's central region in the no-front and front cases.

These mechanisms were most likely not linked to sensible heating from the ground because the variations in the geopotential were out of phase with the temperature variations.

3.3. Moisture Transport and Rainfall

Figures 6 and 7 show the magnitude of the vertically integrated moisture transport for both cases, as well as the wind vectors. A comparison of all panels in both figures shows

that for both cases, subtropical transport peaked in the cool hours, especially at 12Z, in phase with the wind magnitude and zonal component of the gradient of the geopotential at low levels. The no-front case shows strong southeastward transport in the deep tropics north of 21° S. Subtropical moisture transport was more intense in the front case in two ways: it attained higher values, surpassing $800 \text{ kg m}^{-1} \text{ s}^{-1}$ compared to the $600 \text{ kg m}^{-1} \text{ s}^{-1}$ of the no-front case, and a much larger area was covered by transport with magnitude values above $400 \text{ kg m}^{-1} \text{ s}^{-1}$. This means more moisture was carried southwards by the flow than in the no-front case. Plates E and F in Figure 7 show very strong moisture transport south of 33° S, but a comparison with plates E and F in Figure 3 reveals that this was west of the transient trough and not related to the NAL.

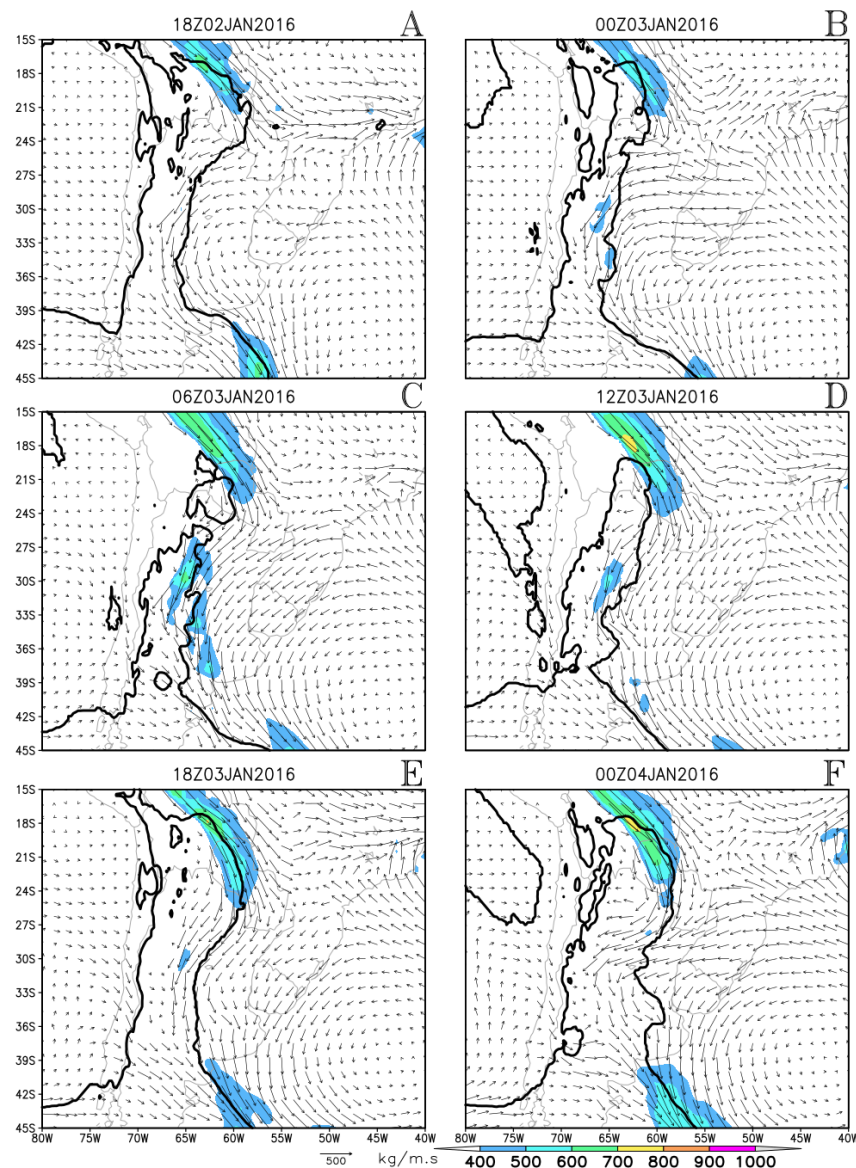


Figure 6. No-front case: Magnitude of the vertically integrated moisture transport. Values above $400 \text{ kg m}^{-1} \text{ s}^{-1}$ are indicated by colors. Vertically integrated moisture transport [$\text{kg m}^{-1} \text{ s}^{-1}$] is indicated by arrows. For reference, the low-pressure tongue east of the Andes is indicated by the actual geopotential height contours. Panels (A–F) show different times, as specified above each panel.

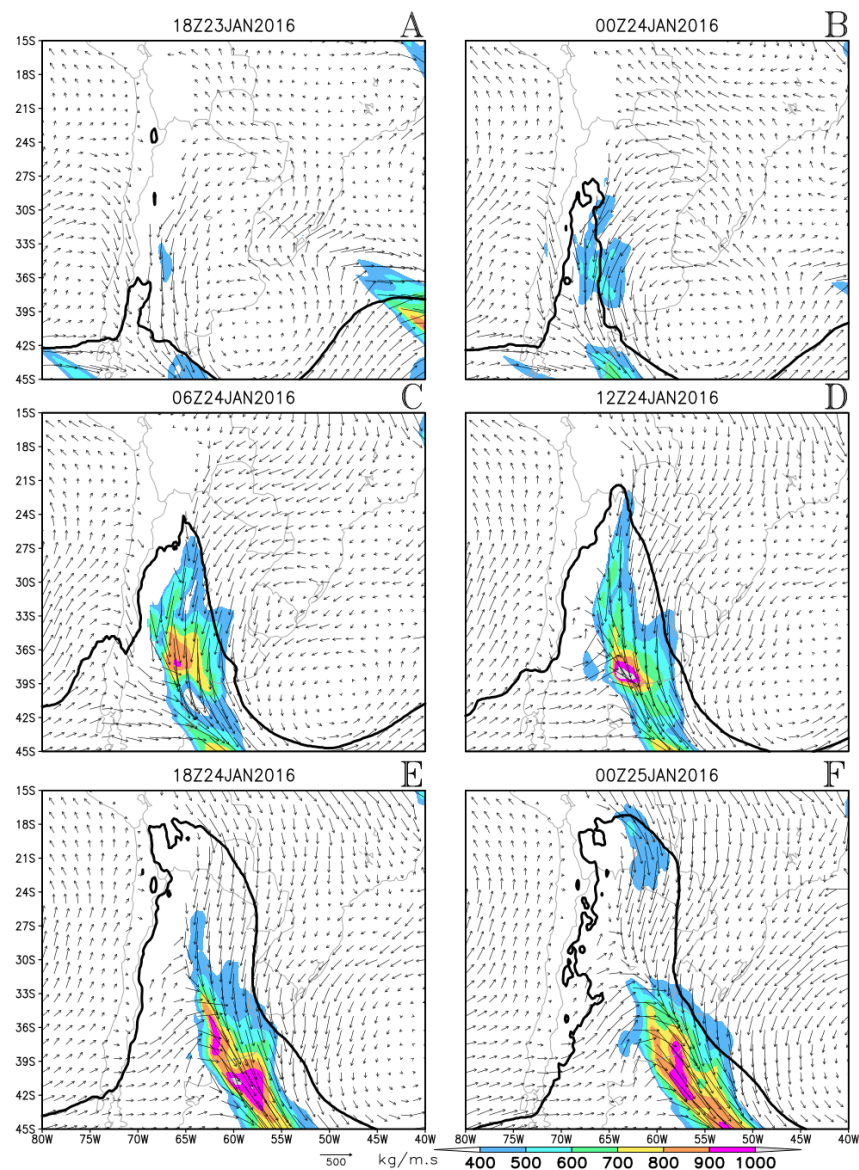


Figure 7. As in Figure 6 but for the front case.

Figures 8 and 9 show the precipitation rates at six-hour intervals for the no-front and front cases, whereas Figures 10 and 11 show the infrared satellite imagery at the closest possible hours. The front case shows a diagonal band of precipitation and low-cloud top temperatures along the frontal zone, spanning latitudes from 42° S to 32° S (Figure 9C,D). There is a maximum at the Argentinean Col, as also observed in [6]. The rainfall rates were considerably higher in the no-front case, despite its weaker moisture transport. These rates rose above 65 mm of accumulated rainfall over six hours, as seen in plates C, D, and E in Figure 8. Meanwhile, in the front case, the rainfall rates were mainly between 15 mm and 55 mm accumulated over six hours. A simple visual analysis of the satellite imagery suggests more convective cloudiness in the no-front case (Figure 10, Plates B, C, and D). The field of equivalent potential temperature shown in Figures 12 and 13, points to a possible explanation.

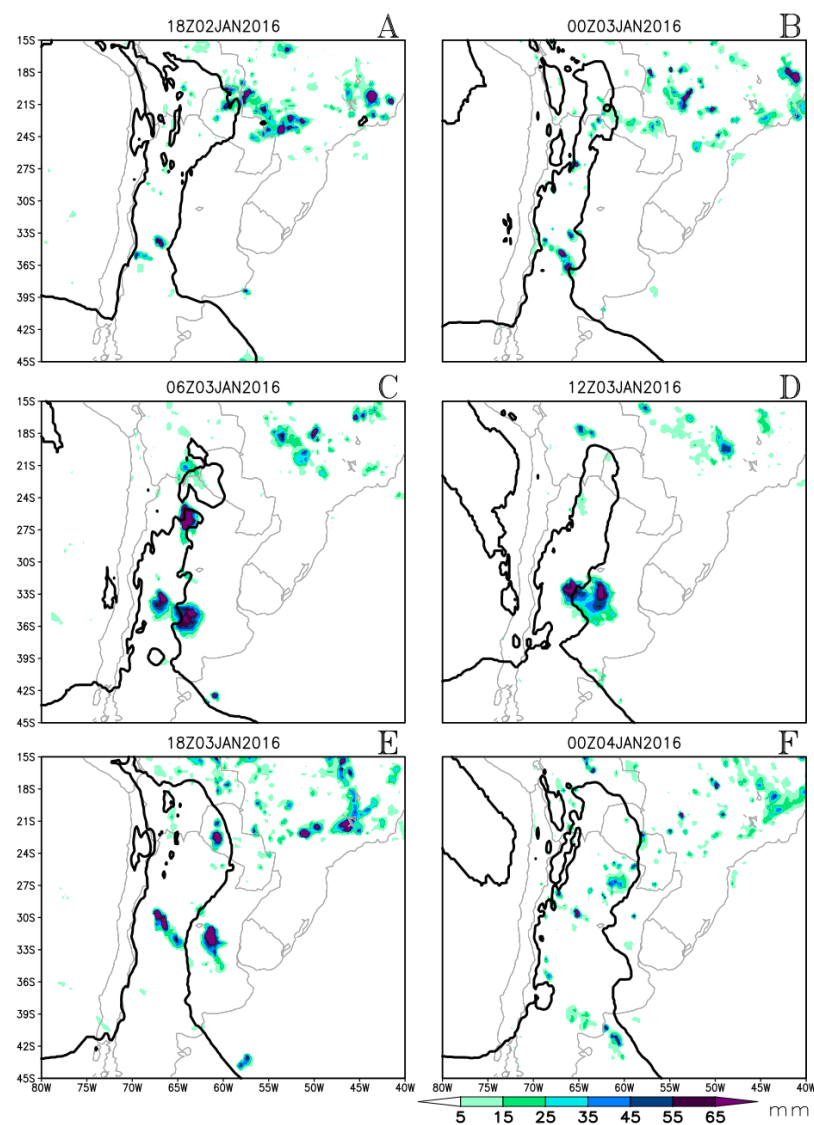


Figure 8. No-front case: Six-hour accumulated precipitation (colors). For reference, the low-pressure tongue east of the Andes is indicated by the actual geopotential height contours. Panels (A–F) show different times, as specified above each panel.

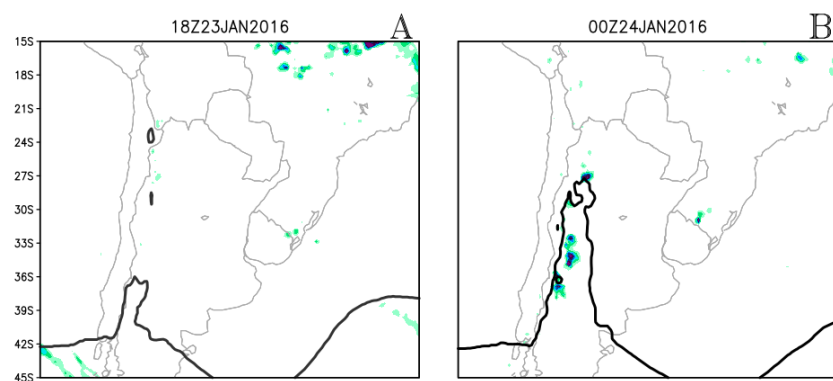


Figure 9. Cont.

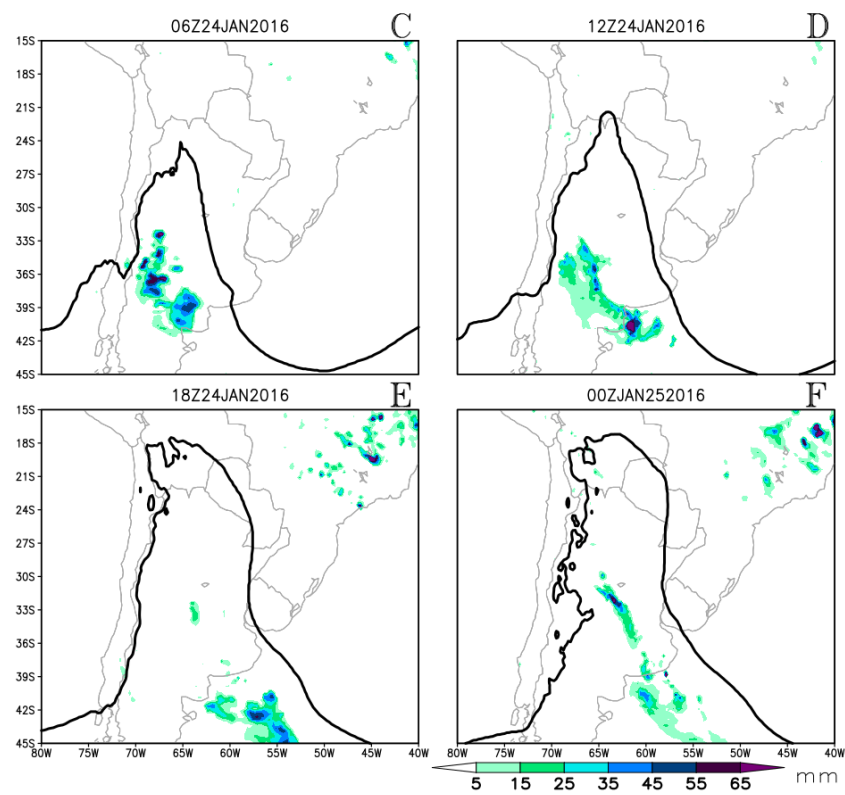


Figure 9. As in Figure 8 but for the front case.

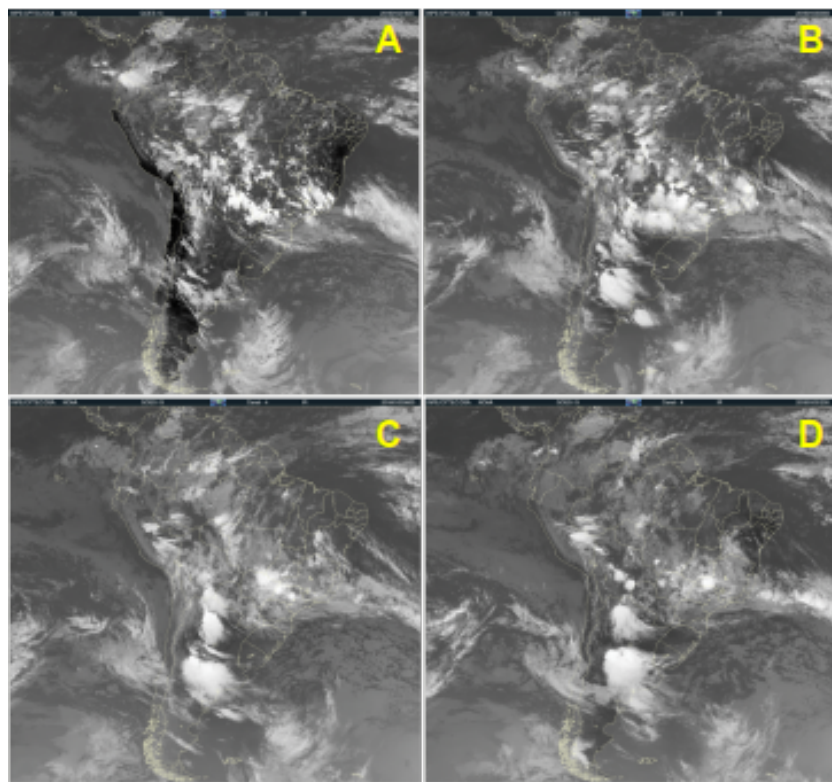


Figure 10. Cont.

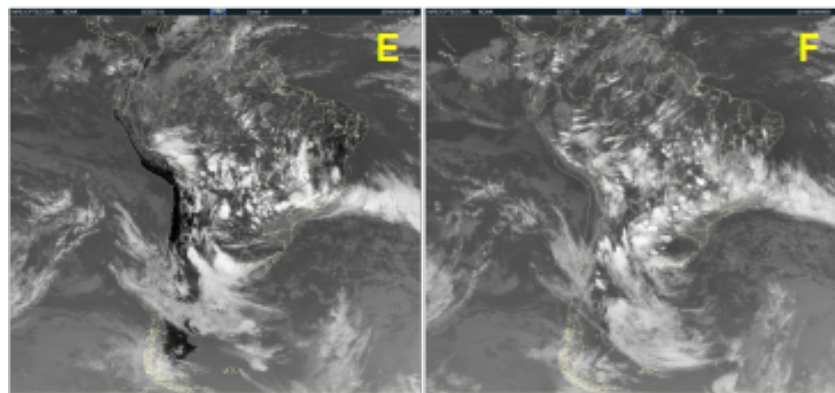


Figure 10. No-front case: Satellite images from the IR-4 channel. All panels show 18Z, on 2 January 2016 (A) to 00Z (03 LST) on 4 January 2016 (F). The time goes from left to right and from top to bottom. The time interval is 6 h. The images were obtained from <http://satelite.cptec.inpe.br/acervo/>, accessed on 18 December 2017. Panels (A–F) show different times, as specified above each panel.

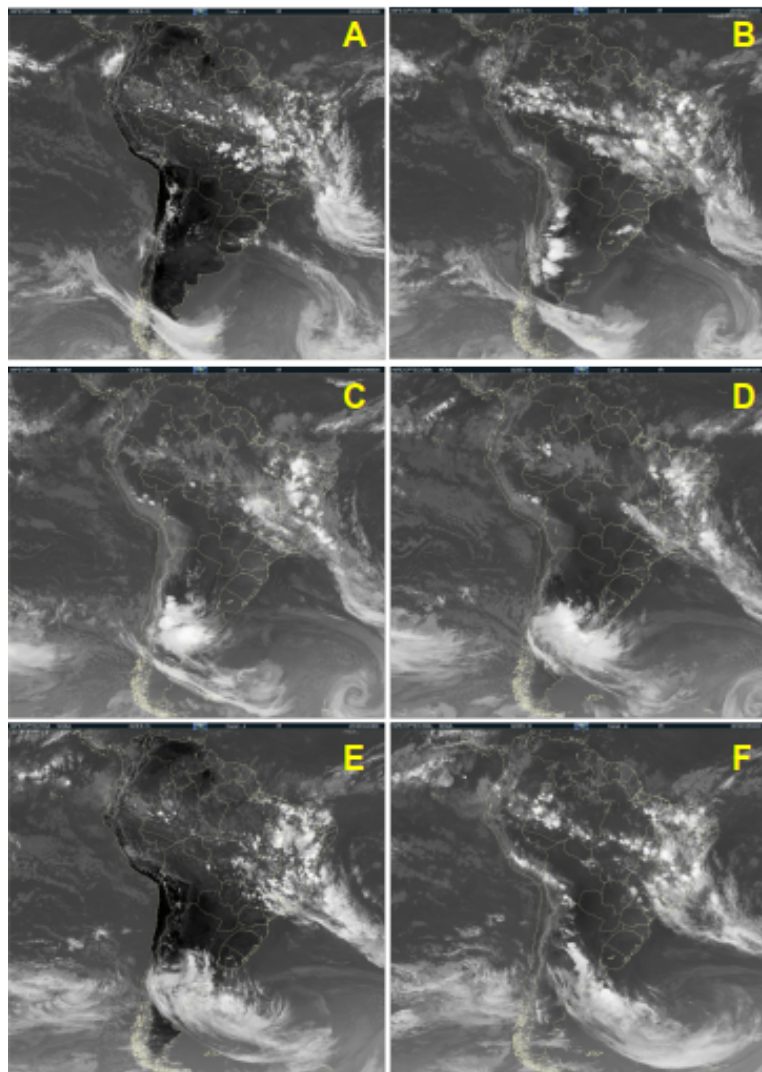


Figure 11. As in Figure 10 but for the front case. Panels (A–F) show different times, as specified above each panel.

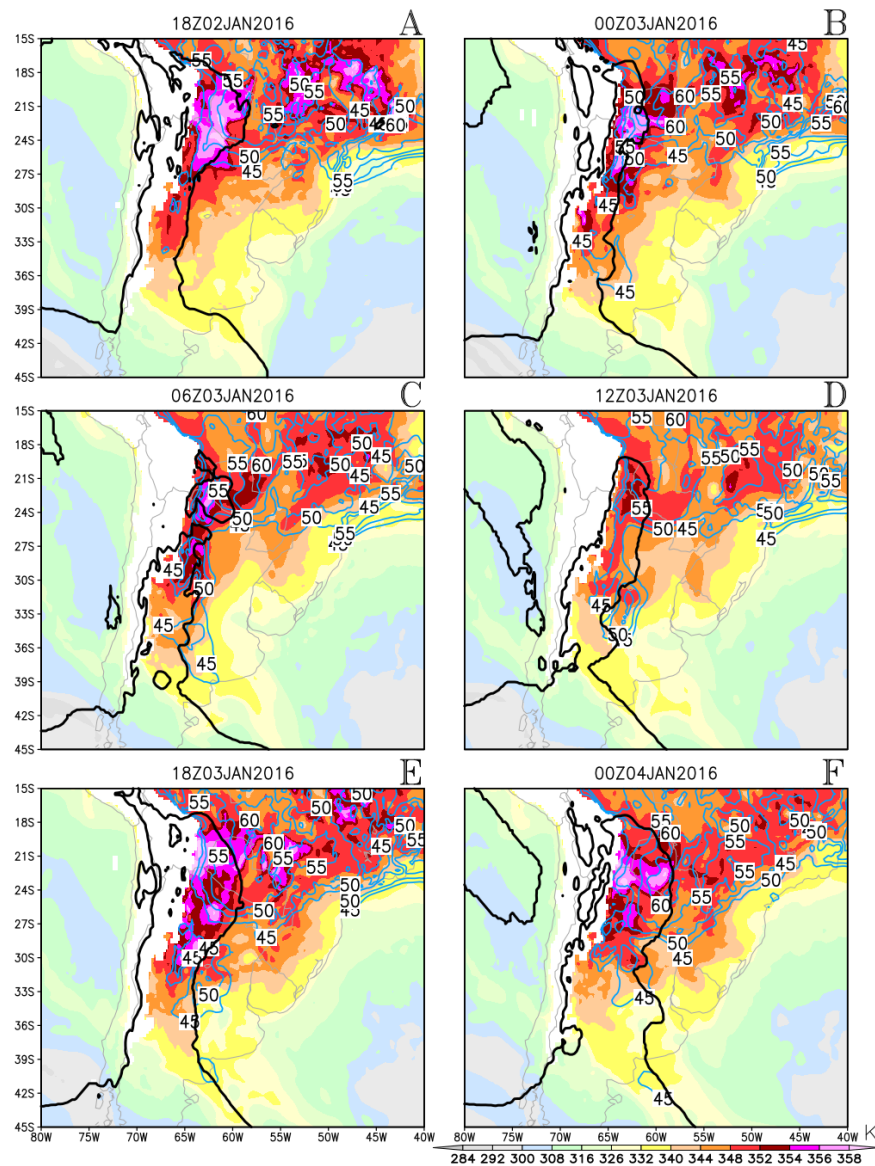


Figure 12. No-front case: Equivalent potential temperature (K) (colors) at 850 mb and the precipitable water with minimal values of 45 mm and an interval of 5 mm (contours). For reference, the low-pressure tongue east of the Andes is indicated by the actual geopotential height contours. Panels (A–F) show different times, as specified above each panel.

The front case shows lower values of the equivalent potential temperature in the subtropics (Figure 13A–F) despite being considerably warmer (Figure 2). Plates A to D in Figure 13 show an area of reduced equivalent potential temperature east of the NAL roughly from 22° S to 30° S, with frontal zones limiting this area to the north and south. The comparison to the field of precipitable water shows that the equivalent potential temperature was lower because the air was drier (Figures 12 and 13). Synoptic analysis of the days prior to the event (Figure 3) revealed that a dry air mass was brought into the subtropics and advected by a transient anti-cyclone. The difference in subtropical moisture between the two cases was not due to the characteristics of the events themselves but rather because of a dry incursion preceding the front case (see Figures 14 and 15 for both cases). A moister band can be seen south of the dry subtropical region, which is located over an area of convergence of the vertically integrated moisture transport (see Figure 15)

and precipitation. This suggests that the vertically integrated moisture flux convergence moistened the air, making it more prone to precipitation.

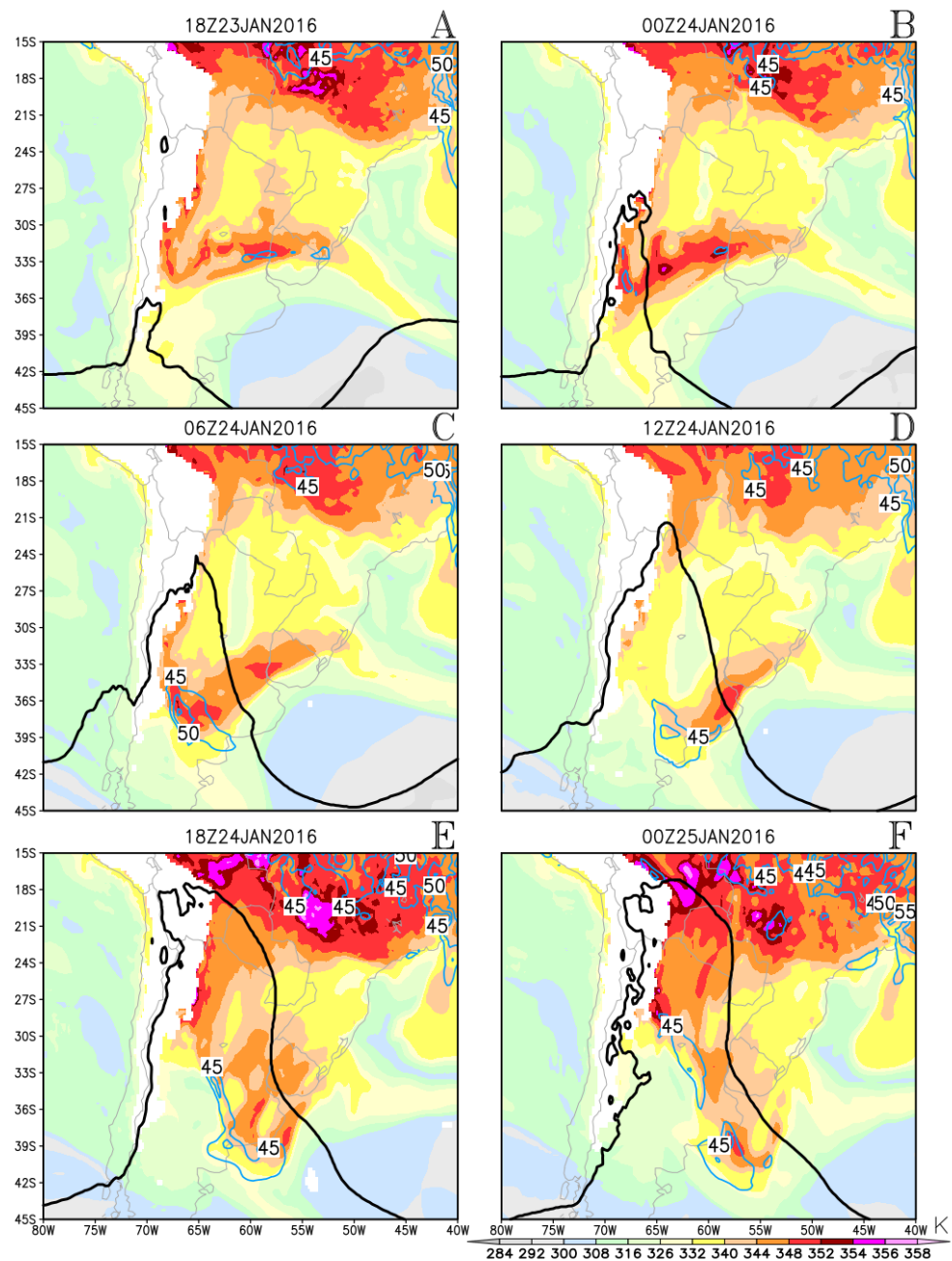


Figure 13. As in Figure 12 but for the front case.

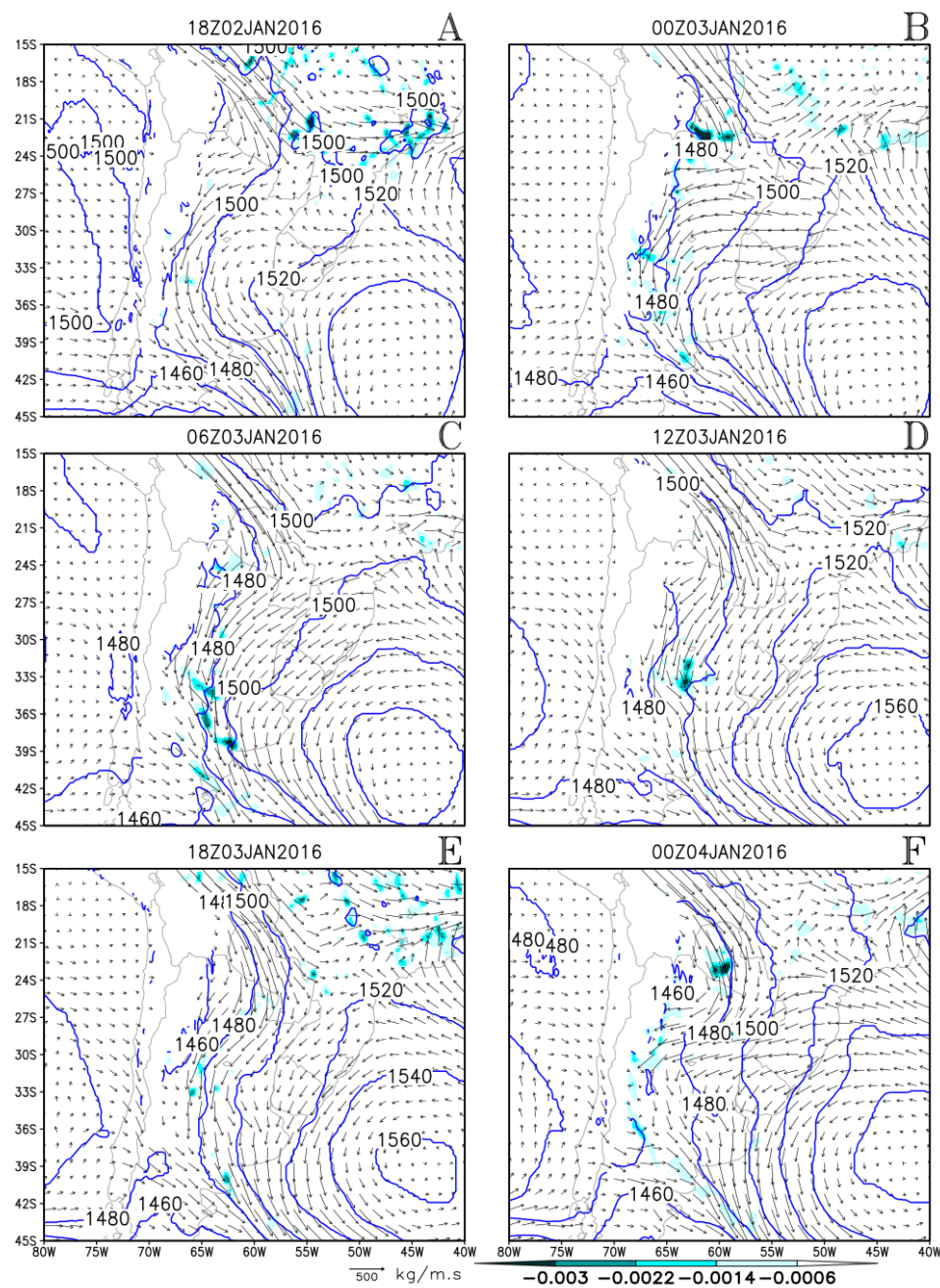


Figure 14. No-front case: Divergence of the vertically integrated moisture transport below $-0.6 \times 10^{-3} \text{ kg m}^{-2} \text{s}^{-1}$ (colors), moisture transport ($\text{kg m}^{-1} \text{s}^{-1}$) (arrows), and the geopotential height with an interval of 20 m (contours) at 850 mb. Panels (A–F) show different times, as specified above each panel.

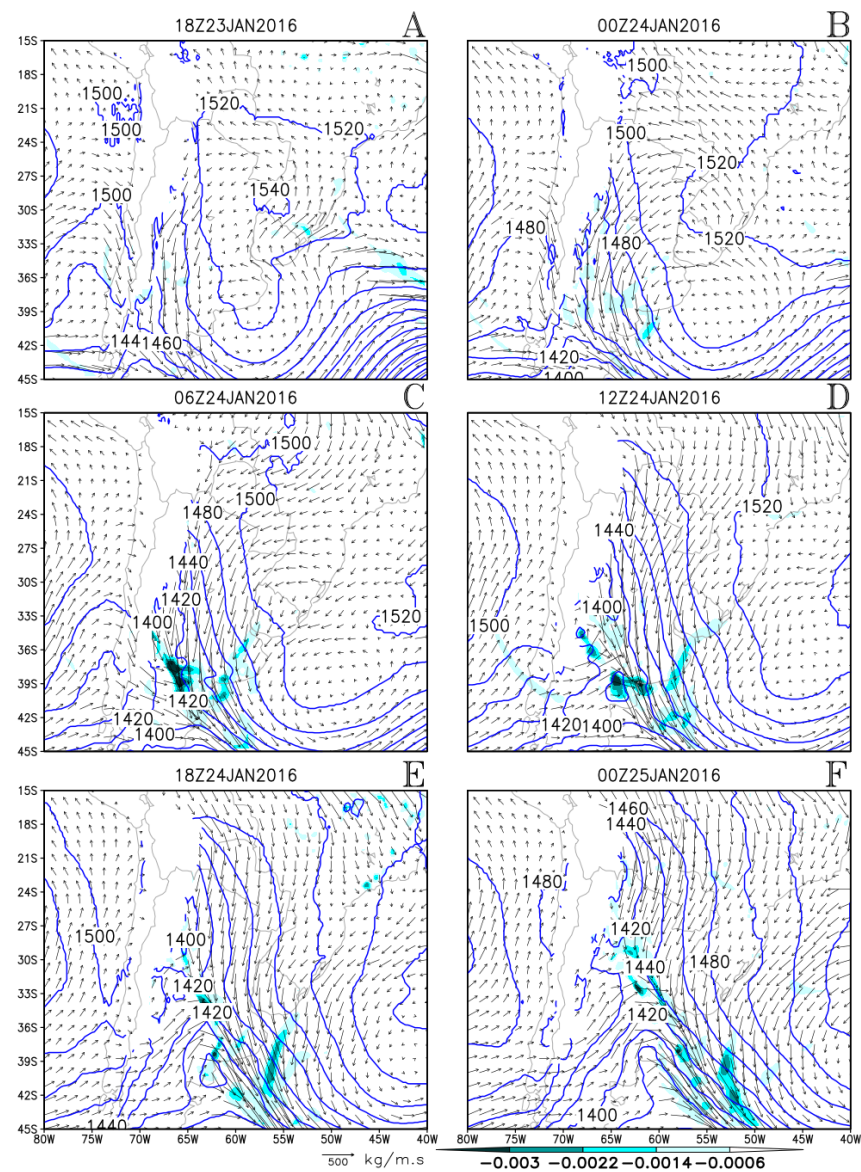


Figure 15. As in Figure 14 but for the front case.

4. Discussions, Summary, and Further Studies

This work analyzes two NAL situations: one coupled to a transient trough and a cold front to its south and another without this coupling. The cold front, which is embedded in the transient trough, shows heavy precipitation fed by moisture transport from the tropics. This moisture transport is enhanced by geostrophic adjustment with the eastern branch of the NAL. When the western branch of the transient trough reaches the continent east of the Andes, the dry and cold southwesterlies flowing west of the trough axis flow into the warm and moist subtropics, resulting in cold advection and frontogenesis, especially in the equivalent potential temperature (see [6]). In this baroclinic environment, the transient trough intensifies and grows, causing the southwesterly flow west of the trough axis to advance northeastward, bringing cold advection that begins to dissipate the NAL from the south.

The front case is warmer than the no-front case and remains warmer than its surroundings throughout the night. The no-front case blends with its surroundings during the night. For the front case, the geopotential falls throughout the night despite the cooling. This may indicate a dynamical mechanism at play.

The front case shows a much more intense zonal component of the geopotential gradient, wind, and moisture transport magnitudes east of the NAL. However, both cases show peaks in the zonal component of the geopotential gradient, wind magnitude, and vertically integrated moisture transport magnitude at 850 mb east of the NAL at 12Z and at 06Z (9 a.m and 3 a.m local times, Figures 4–9). This is consistent with previous studies that show that the SALLJ, an intense tropical moisture flow, and the CHJ peaked at night [26–28].

The rainfall rates are considerably higher in the no-front case (compare Figures 8C,D and 9) despite the much weaker moisture transport. The no-front case shows a typically subtropical behavior, with a mesoscale convective system forming in the exit region of the tropical moisture flow. The front case shows typical extratropical behavior, with rainfall over the front and a maximum over the Argentinean Col. Moisture convergence at the Argentinean Col and the front moistens the atmosphere. The equivalent potential temperature is lower in the subtropics in the front case, even though the temperature is higher. This happens because the air is drier. It is verified (not shown) that the lower values of precipitable water in the front case were due to an incursion of dry air from higher latitudes that occurred in the previous days. Figures 12–15 indicate that convergence of the vertically integrated moisture transport played a central role in moistening the atmosphere and rendering it prone to rainfall in the front case, whereas it did not play the same role in the no-front case. This will be the subject of further research. Two hypotheses are proposed for future study:

1. Drying in the low levels stabilizes the atmosphere, either by reducing the Convective Available Potential Energy or by increasing the Convective Inhibition (CIN), or possibly both.
2. The convergence of the vertically integrated moisture transport at the frontal area south of the NAL has a double role: (i) it moistens the atmosphere, thus generating the CAPE and reducing the CIN, and (ii) It provides a forcing for vertical motion, allowing the air to overcome the CIN.

Another interesting point for further consideration is the geostrophic adjustment at the eastern branch of the NAL. Firstly, there is an extensive meridional flow, often spanning more than 20° S latitude, located in the tropics and subtropics, where the variation of the Coriolis parameter with latitude is high compared to the mid-latitudes (proportional to the cosine of latitude). This means that the Coriolis parameter undergoes considerable changes throughout the flow. Secondly, there is the issue of the nocturnal maximum of the zonal gradient of the geopotential at the western flank of the NAL. This trait was common to both studied events, showing that it has some degree of independence relative to the intensity of the NAL at its center.

Climate change projections show reduced rainfall on the equatorward side of monsoonal regions and increased rainfall on their poleward side. Horizontal moisture transport, including poleward transport from the tropics, is projected to increase [29]. For these reasons, it is likely that the rainfall events described in this work will become more intense in a warmer climate.

Author Contributions: J.M.A. and M.R.R. were involved in all aspects of paper production: conceptualization, methodology, software, formal analysis and visualization. E.P.S. contributed with Conceptualization and formal analysis. J.A.N. contributed with formal analysis, software and visualization. All authors have read and agreed to the published version of the manuscript.

Funding: This research was funded by National Council for Scientific and Technological Development (CNPq) grant number 131580/2016-7.

Institutional Review Board Statement: Not applicable.

Informed Consent Statement: Not applicable.

Data Availability Statement: All data used in this paper are publicly available on the following platforms: <https://cds.climate.copernicus.eu/>, <https://trmm.gsfc.nasa.gov/>, and <https://www.cptec.inpe.br/>, accessed on 24 December 2022, 12 December 2017, and 18 December 2017, respectively.

Acknowledgments: The authors thank National Council for Scientific and Technological Development (CNPq) for financial support and the Federal University of Campina Grande and the University of São Paulo.

Conflicts of Interest: The authors declare no conflict of interest.

Abbreviations

The following abbreviations are used in this manuscript:

NAL	Northwestern Argentinean Low
CHJ	Chaco Jet
SALLJ	South America Low-Level Jet
BCH	Chaco Low
CIN	Convective Inhibition
TRMM	Tropical Rainfall Measuring Mission
UTC	Universal Time Coordinated
SACZ	South Atlantic Convergence Zone
SASH	South Atlantic Subtropical High
ECMWF	European Centre for Medium-Range Weather Forecasts

References

1. Zhou, J.; Lau, K.-M. Does a Monsoon Climate Exist over South America? *J. Clim.* **1998**, *11*, 1020–1040. [[CrossRef](#)]
2. Marengo, J.A.; Liebmann, B.; Grimm, A.M.; Misra, V.; Silva Dias, P.L.; Cavalcanti, I.F.A.; Carvalho, L.M.V.; Berbery, E.H.; Ambrizzi, T.; Vera, C.S.; et al. Recent developments on the South American monsoon system. *Int. J. Climatol.* **2010**, *32*, 1–21. [[CrossRef](#)]
3. Schwerdtfeger, W. Climates of Central and South America. In *World Survey of Climatology*; Elsevier: Amsterdam, The Netherlands, 1976; Volume 12, pp. 1–145.
4. Seluchi, M.E.; Saulo, A.C.; Nicolini, M.; Satyamurty, P. The Northwestern Argentinean Low: A Study of Two Typical Events. *Mon. Weather. Rev.* **2003**, *131*, 2361–2378. [[CrossRef](#)]
5. Seluchi, M.E.; Garreaud, R.D. Campos médios e processos físicos associados ao ciclo de vida da Baixa do Chaco. *Rev. Bras. Meteorol.* **2012**, *27*, 447–462. [[CrossRef](#)]
6. Arraut, J.M. Fronts and Frontogenesis during Summer: Geometrical and Dynamical Aspects and the Influence over Rainfall on the South American Subtropics. Ph.D Thesis, Centro de Previsão de Tempo e Estudos Climáticos—INPE, São Paulo, Brazil, 2007.
7. Ferreira, L.J. Causas y Variabilidad de la Depresión del Noroeste Argentino e Impactos sobre los Patrones Regionales de Circulación. Ph.D Thesis, Universidad de Buenos Aires, Buenos Aires, Argentina, 2008.
8. Escobar, G.C.J. Classificação sinótica dos campos de pressão atmosférica na América do Sul e sua relação com as baixas do Chaco e do Noroeste Argentino. *Rev. Bras. Meteorol.* **2012**, *27*, 365–375. [[CrossRef](#)]
9. Seluchi, M.E.; Saulo, A.C. Baixa do Noroeste Argentino e Baixa do Chaco: características, diferenças e semelhanças. *Rev. Bras. Meteorol.* **2012**, *27*, 49–60. [[CrossRef](#)]
10. Seluchi, M.E.; Norte, F.A.; Satyamurty, P.; Chou, S.C. Analysis of Three Situations of the Foehn Effect over the Andes (Zonda Wind) Using the Eta-CPTEC Regional Model. *Weather. Forecast.* **2003**, *18*, 481–501. [[CrossRef](#)]
11. Lemenkova, P. Comparative analysis of climate and topography in Chaco and Oriental Paraguay. *Cad. Geogr.* **2021**, *31*, 865–888. [[CrossRef](#)]
12. Ferreira, G.W.S.; Reboita, M.S. A New Look into the South America Precipitation Regimes: Observation and Forecast. *Atmosphere* **2022**, *13*, 873. [[CrossRef](#)]
13. Salio, P.; Nicolini, M.; Saulo, A.C. Chaco low-level jet events characterization during the austral summer season. *J. Geophys. Res. Atmos.* **2002**, *107*, ACL–32. [[CrossRef](#)]
14. Saulo, A.C.; Seluchi, M.E.; Nicolini, M. A Case Study of a Chaco Low-Level Jet Event. *Mon. Weather. Rev.* **2004**, *132*, 2669–2683. [[CrossRef](#)]
15. Salio, P.; Nicolini, M.; Zipser, E. Mesoscale Convective Systems over Southeastern South America and Their Relationship with the South American Low-Level Jet. *Mon. Weather. Rev.* **2007**, *135*, 1290–1309. [[CrossRef](#)]
16. Mendes, D.; Souza, E.P.; Trigo, I.F.; Mir, P.M.A. On precursors of South American cyclogenesis. *Tellus A Dyn. Meteorol. Oceanogr.* **2007**, *59A*, 114–121. [[CrossRef](#)]
17. Barbosa, H.M.J.; Arraut, J.M. A quantitative evaluation of the role of the Argentinean Col and the Low Pressure Tongue East of the Andes for frontogenesis in the South American subtropics. *Adv. Geosci.* **2009**, *22*, 67–72. [[CrossRef](#)]
18. Arraut, J.M.; Barbosa, H.M.J. Large scale features associated with strong frontogenesis in equivalent potential temperature in the South American subtropics east of the Andes. *Adv. Geosci.* **2009**, *22*, 73–78. [[CrossRef](#)]
19. Arraut, J.M.; Satyamurty, P. Precipitation and water vapor transport in the Southern Hemisphere with emphasis on the South American region. *J. Appl. Meteorol. Climatol.* **2009**, *48*, 1902–1912. [[CrossRef](#)]

20. Reboita, M.S.; Kuki, C.A.C.; Marrafon, V.H.; de Souza, C.A.; Ferreira, G.W.S.; Teodoro, T.; Lima, J.W.M. South America climate change revealed through climate indices projected by GCMs and Eta-RCM ensembles. *Clim. Dyn.* **2022**, *58*, 459–485. [[CrossRef](#)]
21. Almazroui, M.; Ashfaq, M.; Islam, M.N.; Rashid, I.U.; Kamil, S.; Abid, M.A.; O'Brien, E.; Ismail, M.; Reboita, M.S.; Sörensson, A.A.; et al. Assessment of CMIP6 Performance and Projected Temperature and Precipitation Changes Over South America. *Earth Syst. Environ.* **2021**, *5*, 155–183. [[CrossRef](#)]
22. Llopis, M.; Coppola, E.; Giorgi, F.; da Rocha, R.P.; Cuadra, S.V. Climate change impact on precipitation for the Amazon and La Plata basins. *Clim. Chang.* **2014**, *125*, 111–125. [[CrossRef](#)]
23. Pascale, S.; Carvalho, L.M.V.; Adams, D.K.; Castro, C.L.; Cavalcanti, I.F.A. Current and Future Variations of the Monsoons of the Americas in a Warming Climate. *Curr. Clim. Chang. Rep.* **2019**, *5*, 125–144. [[CrossRef](#)]
24. Nielsen, D.M.; Cataldi, M.; Belém, A.L.; Albuquerque, A.L.S. Local indices for the South American monsoon system and its impacts on Southeast Brazilian precipitation patterns. *Nat. Hazards* **2016**, *83*, 909–928. [[CrossRef](#)]
25. Bolton, D. The computation of Equivalent Potential Temperature. *Mon. Weather. Rev.* **1980**, *108*, 1046–1053. [[CrossRef](#)]
26. Garreaud, R.D.; Wallace, J.M. The Diurnal March of Convective Cloudiness over the Americas. *Mon. Weather. Rev.* **1997**, *125*, 3157–3171. [[CrossRef](#)]
27. Vernekar, A.D.; Kirtman, B.P.; Fennessy, M.J. Low-level jets and their effects on the South American summer climate as simulated by the NCEP Eta Model. *J. Clim.* **2003**, *16*, 297–311. [[CrossRef](#)]
28. Marengo, J.A.; Soares, W.R.; Saulo, C.; Nicolini, M. Climatology of the Low Level Jet East of the Andes as derived from the NCEP-NCAR reanalyses: characteristics and temporal variability. *J. Clim.* **2004**, *17*, 2261–2280. [[CrossRef](#)]
29. Held, I.M.; Soden, B.J. Robust Responses of the Hydrological Cycle to Global Warming. *J. Clim.* **2006**, *19*, 5686–5699. [[CrossRef](#)]

Disclaimer/Publisher's Note: The statements, opinions and data contained in all publications are solely those of the individual author(s) and contributor(s) and not of MDPI and/or the editor(s). MDPI and/or the editor(s) disclaim responsibility for any injury to people or property resulting from any ideas, methods, instructions or products referred to in the content.